nanotechweb.org

LAB TALK

Aug 13, 2014

Tuning the magnetic properties of bimagnetic core/shell nanoparticles

Designing multi-phase transition metal oxide nanoparticles could be promising in the development of new rare-earth-free permanent magnets and high-density data-storage devices. Reporting in *Nanotechnology* (http://iopscience.iop.org/0957-4484/25/35/355704/), researchers at the Bariloche Atomic Centre in Argentina design and fabricate antiferromagnetic CoO nanoparticles encapsulated in a ferrimagnetic $CoFe_2O_4$ shell. They show that the magnetic hardness and the magnetic thermal stability can be successfully increased by the exchange coupling at the interface. Moreover, the magnetic properties can be tuned by changing the characteristic sizes of the core/shell structure.

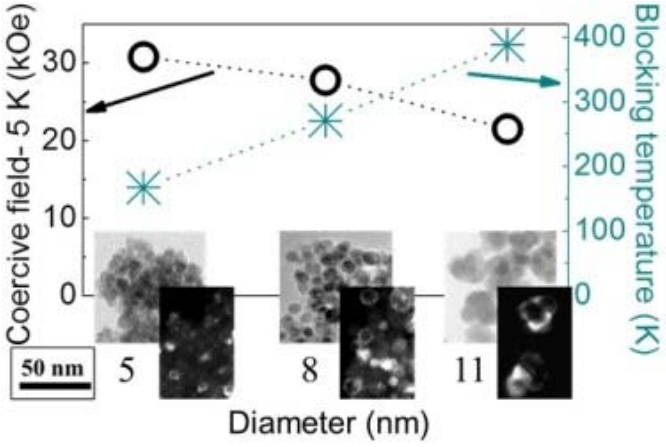

(http://images.iop.org/objects/ntw/journal/13/8/5/figure1.jpg)
The effect of nanoparticle diameter on the coercive field and blocking temperature (http://images.iop.org/objects/ntw/journal/13/8/5/figure1.jpg)

Novel permanent magnets and high-density data-storage applications require highly anisotropic materials. Here, researchers show that the effective magnetic anisotropy can be enhanced by the exchange coupling at the interface of bimagnetic nanostructures. When the mean size of $CoO/CoFe_2O_4$ nanoparticles is reduced from 11 to 5 nm, a remarkable increase of the low-temperature coercive field from 21.5 to 30.8 kOe is observed. This is at the expense of a lower blocking temperature.

DC magnetic measurements as well as X-ray powder diffraction (XRD) and transmission electron microscopy (TEM) experiments are carried out in order to study the relationship between the structure and the magnetic properties. A phenomenological model is used to interpret the interplay of the different competing factors on the magnetic hardening. This comprehension is essential for designing and engineering new materials to improve the performance of modern magnetic devices.

The researchers presented their work in the journal *Nanotechnology* **25 355704** (http://iopscience.iop.org/0957-4484/25/35/355704/).

Further reading

Heat-assisted magnetic recording doubles hard disk drive capacity (June 2014) (http://nanotechweb.org/cws/article/lab/57685)

Competing interactions and stepwise magnetization observed in Fe nanoparticle films (Aug 2013) (http://nanotechweb.org/cws/article/lab/54234)
Making monodisperse FeCo nanoparticles the easy way (Oct 2013) (http://nanotechweb.org/cws/article/lab/54894)

About the author

Gabriel Lavorato (http://fisica.cab.cnea.gov.ar/resonancias/paginas-personales/gabriel-c-lavorato) is a PhD candidate at the Balseiro Institute in the Magnetic Resonance Laboratory (http://fisica.cab.cnea.gov.ar/resonancias/) of the Bariloche Atomic Centre in Argentina, supervised by Elin Winkler (http://fisica.cab.cnea.gov.ar/resonancias/paginas-personales/elin-winkler) and Roberto Zysler (http://fisica.cab.cnea.gov.ar/resonancias/paginas-personales/roberto-zysler). His research is devoted to the synthesis and study of bimagnetic nanoparticles within a group whose main activities cover basic research and the development of new magnetic materials with potential applications by means of different experimental techniques. This work was conducted in close collaboration with Enio Lima Jr (http://fisica.cab.cnea.gov.ar/resonancias/paginas-personales/enio-lima-jr), Dina Tobia and Horacio Troiani (http://fisica.cab.cnea.gov.ar/metales/es/integrantes/16) from the Bariloche Atomic Centre in Argentina and Dino Fiorani (http://www.ism.cnr.it/english/staff/fioranid.php) from the Institute of Structure of Matter of the Italian National Research Council in Italy.

IOP Publishing Nanotechnology
Nanotechnology **25** (2014) 355704 (9pp) doi:10.1088/0957-4484/25/35/355704

Size effects in bimagnetic $CoO/CoFe_2O_4$ core/shell nanoparticles

Gabriel C Lavorato[1,2], Enio Lima Jr[1,2], Dina Tobia[1,2], Dino Fiorani[2,3], Horacio E Troiani[1], Roberto D Zysler[1,2] and Elin L Winkler[1,2]

[1] Centro Atómico Bariloche, CNEA-CONICET, 8400 S.C. de Bariloche, Río Negro, Argentina
[2] Argentine-Italian Joint Laboratory of Nanomagnetism, LIANAM, Laboratorio Resonancias Magnéticas –CNEA, Argentina/Istituto di Struttura della Materia, CNR, Italy
[3] Istituto di Struttura della Materia, CNR, Area della Ricerca di Roma, C.P. 10, I-00016 Monterotondo Staz., Rome, Italy

E-mail: lavorato@cab.cnea.gov.ar

Received 18 April 2014, revised 9 July 2014
Accepted for publication 17 July 2014
Published 13 August 2014

Abstract

The control of the size of bimagnetic nanoparticles represents an important step toward the study of fundamental properties and the design of new nanostructured magnetic materials. We report the synthesis and the structural and magnetic characterization of bimagnetic $CoO/CoFe_2O_4$ core/shell nanoparticles. The material was fabricated by a seed-mediated growth high-temperature decomposition method with sizes in the range of 5–11 nm. We show that the core/shell morphology favours the crystallinity of the shell phase, and the reduction of the particle size leads to a remarkable increase of the magnetic hardening. When the size is reduced, the coercive field at 5 K increases from 21.5 kOe to 30.8 kOe, while the blocking temperature decreases from 388 K to 167 K. The size effects on the magnetic behaviour are described through a phenomenological model for strongly ferri-/antiferromagnetic coupled phases.

Keywords: bimagnetic nanoparticles, magnetic anisotropy, interface exchange coupling, cobalt ferrite, nanomagnetism

(Some figures may appear in colour only in the online journal)

1. Introduction

The fabrication of artificial nanostructures and the advance of physical properties' detection techniques allow the study of fundamental properties at the nanoscale level and drive the development of new applications [1–3]. In the case of magnetic nanoparticles, the search for new materials for the development of advanced magnets and high density data storage is an area of great interest [4, 5]. However, it is well known that when the size of the particle is reduced beyond the superparamagnetic threshold, the nanoparticle magnetic moment fluctuates [6, 7]. As a consequence, the research is oriented to the production of highly anisotropic materials to increase the magnetic moment thermal stability. Most of these single-phase high-performance materials are expensive, such as FePt, or are based on limited rare earth compounds, such as $Nd_2Fe_{14}B$ or $SmCo_5$ [8–11]. Another potential approach is the design and fabrication of bimagnetic transition metal oxide nanoparticles, which exploit the properties of each phase and the interface exchange interaction. Thermal decomposition methods allow the fabrication of nanoparticles with controlled size and composition [12, 13] and high-quality bimagnetic core/shell nanoparticles have been obtained through seed-mediated growth [8, 14–18]. The core/shell nanoparticles could improve the performance of modern permanent magnets by increasing the effective magnetic anisotropy of the material through the coupling between the different magnetic phases. However, few examples of structures with different core/shell compositions were reported, i.e., $CoFe_2O_4/MnO$ [19], $FeO/CoFe_2O_4$ [14], $CoFe_2O_4/CoFe_2$ [20, 21], Co/MFe_2O_4 (M = Mn, Fe) [15] and Fe_3O_4/Mn_3O_4 [22]. Since comprehensive theories that account for the magnetic behaviour of core/shell bimagnetic nanoparticles are still lacking, our investigation aimed to understand the size effects on the magnetic properties of bimagnetic systems that are of crucial importance for designing and engineering new

Table 1. Synthesis conditions and structural parameters: reflux temperature (T_{REFLUX}); heating rate of the first step (*HR*); surfactant/precursor molar ratio (*S*/*P*); mean core diameter ($<D_{CORE}>$); mean particle diameter ($<D_{NP}>$) and its standard deviation (σ_D), measured by TEM; mean size of CoO $<D_{CoO}>$ and $CoFe_2O_4$ $<D_{CoFeO}>$ phases estimated by XRD.

	Synthesis parameters			TEM			XRD	
	T_{REFLUX}	*HR*	*S*/*P*	$<D_{CORE}>$	$<D_{NP}>$	σ_D	$<D_{CoO}>$	$<D_{CoFeO}>$
Sample	(°C)	(°C min^{-1})	(mol mol^{-1})	(nm)	(nm)	(nm)	(nm)	(nm)
S1	255	5	4	2.6	5.1	0.9	2	4.5
S2	255	30	4	3.8	8.2	1.2	6	6
S3	285	30	2	6.0	11.3	1.7	—	14

materials. Recently, it has been found that CoO/$CoFe_2O_4$ core/shell nanoparticles that combine two highly anisotropic magnetic materials show a remarkable increase of coercivity compared to their single-phase parent compounds [23]. The origin of this magnetic hardening was associated with the exchange coupling between the antiferromagnetic core and the ferrimagnetic shell [24] and, being an interface phenomenon, it should be strongly dependent on the size of the particles. When the nanoparticle size is reduced, the crystalline and magnetic disorder increases, and the influence of thermal fluctuations becomes more important. To elucidate the interplay of the different competing factors on the magnetic hardening, we investigated the core/shell samples as a function of the nanoparticle size. In this frame, we synthesized and studied the structural and magnetic properties of CoO nanoparticles with different diameters ranging from 2.6 nm to 6 nm, encapsulated in a $CoFe_2O_4$ shell of ∼1.3–2.6 nm thickness.

2. Experimental details

2.1. Synthesis of bimagnetic nanoparticles

CoO/$CoFe_2O_4$ core/shell nanoparticles of different sizes were synthesized by means of high-temperature decomposition of the metal acetylacetonates, assisted by oleic acid and oleylamine as surfactants [23]. In a typical synthesis (sample S2), 4 mmol of $Co(acac)_2$ were mixed with 8 mmol of oleic acid, 8 mmol of oleylamine, 0.02 mmol of 1–2 octanediol and 235 mmol of diphenyl ether. In order to obtain monodispersed CoO nanoparticles, the mixture was magnetically stirred and heated to the reflux temperature (260 °C) for 120 min with a controlled heating rate of 30 °C min^{-1}. After cooling to room temperature, 0.8 mmol of $Co(acac)_2$ and 1.6 mmol of $Fe(acac)_3$ were added to the mixture, according to the molar composition of the cobalt ferrite. In the same step, 0.02 mmol of 1–2 octanediol, 4 mmol of oleylamine, 4 mmol of oleic acid and 79 mmol of diphenyl ether were added, and the preparation was heated up to 260 °C for another 120 min. In this second stage, the heating rate was fixed at 30 °C min^{-1} in order to avoid the homogeneous nucleation of the spinel phase and to favour the formation of a core/shell structure.

By modifying the heating rate of the first step, the refluxing temperature and the surfactant/precursor ratio, it was possible to obtain nanoparticles of different sizes and morphologies. Sample S1 was prepared following the same procedure described above, but the heating rate during the first step was fixed at 5 °C min^{-1}. Sample S3 was produced in a similar fashion, but we employed a lower surfactant/precursor molar ratio and used benzyl ether as the solvent, leading to a higher reflux temperature of 285 °C (see table 1). During the second stage of the synthesis, the heating rate was fixed at 30 °C min^{-1} for all of the samples.

After the nanoparticles were cooled to room temperature, they were precipitated by centrifugation (14 000 rpm/30 min) and washed several times with a mixture of ethanol and toluene 8:1 with the objective of eliminating the organic coating. After the toluene evaporated, a dry powder was obtained. In order to improve the crystallinity, the samples were heated to 300 °C with a heating rate of 2.5 °C min^{-1} and kept at that temperature for 2 h in an air atmosphere. The obtained dry powder was then mixed with an epoxy resin to prevent the mechanical movement of the nanoparticles during the magnetic characterization.

2.2. Characterization methods

The nanoparticles' crystalline structure was characterized by x-ray powder diffraction (XRD) using a Philips PW3020 diffractometer (CuKα radiation). Rietveld refinements were performed using the Fullprof software [25] and were used to estimate the crystallite mean size. The core/shell morphology was assessed by means of Philips CM200 UT transmission electron microscopy (TEM), which was operated at 200 kV. The crystallinity and morphology of the samples were evaluated by the analysis of high-resolution and dark-field TEM images. The particles' size distribution was evaluated from bright-field and high-resolution TEM images by measuring around 300 particles of each sample. The magnetic behaviour was analyzed using a superconducting quantum interference device (SQUID, Quantum Design) magnetometer with a ±70 kOe maximum applied field in the temperature range of 4–320 K. Magnetization versus temperature experiments were performed following the ZFC (zero field cooling) and FC (field cooling) procedures at an applied field of 100 Oe. Thermoremanent magnetization (TRM) measurements were performed by cooling the sample from 330 to 5 K under a 100 Oe applied field and by subsequently measuring the temperature dependence of the magnetization at a 0 applied field. The magnetic properties were measured in a Faraday balance magnetometer with a 10 kOe maximum applied field from room temperature to 800 K.

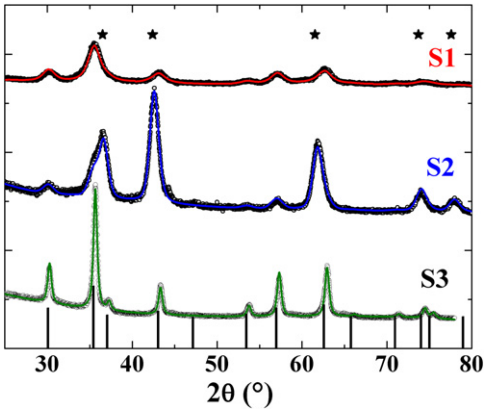

Figure 1. X-ray diffraction patterns and the corresponding Rietveld fits (full lines). The bulk CoO and $CoFe_2O_4$ Bragg positions are indicated with stars (top) and full bars (bottom), respectively.

3. Results and discussion

3.1. Morphology and structural characterization

The x-ray diffraction patterns are presented in figure 1; the Bragg peaks' positions of the bulk CoO and $CoFe_2O_4$ phases are also shown for comparison. Notice that the diffraction peaks that correspond to the $CoFe_2O_4$ phase are clearly detected in all of the systems. However, the contribution of the CoO core phase dominates the diffraction pattern of S2; at plain sight, it cannot be resolved for S1 and S3. Rietveld refinements were performed using the known CoO (JCPDS#43-1004) and $CoFe_2O_4$ (JCPDS#22-1086) bulk crystal structure. The fitting patterns are shown in the full lines in figure 1. The characteristic sizes of the nanostructures were obtained from the fittings. The average crystallite size of the $CoFe_2O_4$ shell (D_{CoFeO}) is 4.5 nm, 6 nm and 14 nm for samples S1, S2 and S3, respectively. Moreover, the average crystallite size for the CoO core (D_{CoO}) resulted in 2 nm for S1 and 6 nm for S2 and could not be resolved for sample S3, probably due to the limited statistic and the different peak broadening of the CoO and $CoFe_2O_4$ phases (see table 1).

Furthermore, the TEM micrographs were analyzed to investigate the size, structure and morphology of the nanoparticles. Figures 2(a)–(c) show the representative images and size dispersion graphs for the three systems. The histograms were constructed according to the Sturges method [26] and were fitted with a lognormal function $f(D) = (1/\sqrt{2\pi}\sigma D)\exp[-\ln^2(D/D_0)/2\sigma^2]$, from which the median diameter D_0 and dispersion σ were estimated. Then, the mean diameter $\langle D\rangle = D_0\exp(\sigma^2/2)$ and standard deviation $\sigma_D = \langle D\rangle[\exp(\sigma^2)-1]^{1/2}$ were calculated (see table 1). The high resolution TEM images presented in figures 3(d)–(f) exhibit a different phase contrast, which unveil the core/shell structure. From these images, the interplanar distances of the phases involved were measured. The value of 4.9 Å shown in figure 3(d) matches well with the (111) $CoFe_2O_4$ plane, while figure 3(f) shows different plane orientations for the inner and outer part of the particle.

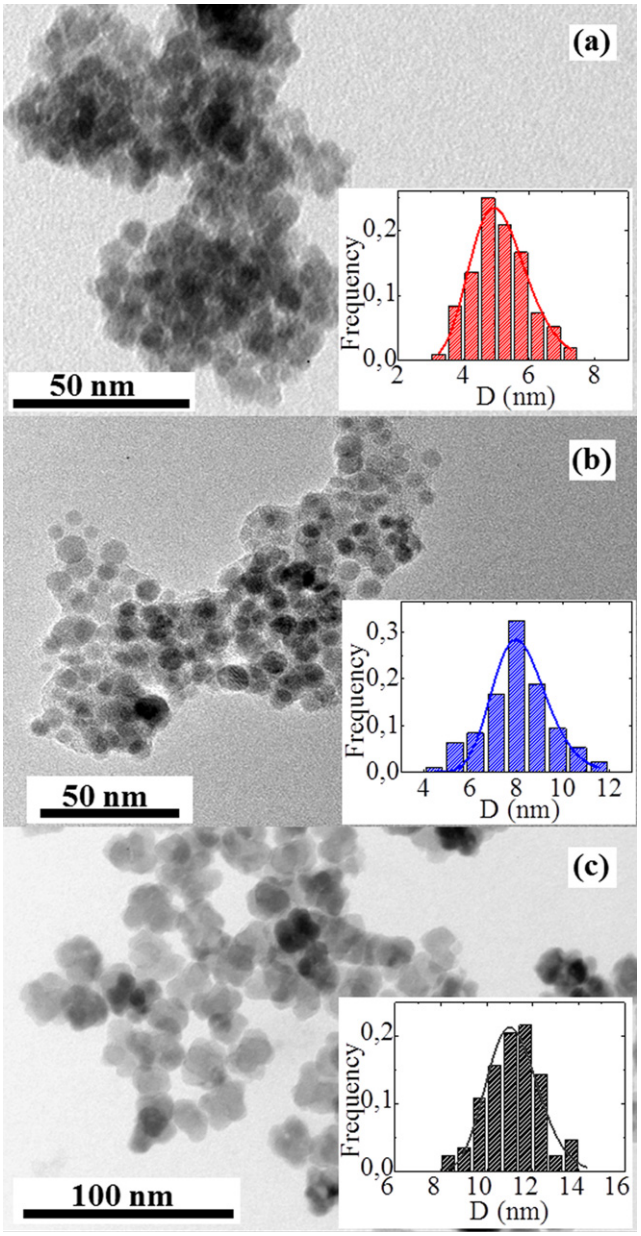

Figure 2. Bright-field TEM images of S1, S2 and S3 CoO-core/$CoFe_2O_4$-shell samples ((a), (b) and (c), respectively). The insets show the diameter distributions and the corresponding lognormal fit.

An enlarged HRTEM image of S3 is shown in figure 4. It is revealed that the interplanar distances measured for the core (figure 4(a)) and the 90° angle between the planes match well with the (1–11) and (110) CoO planes, as shown in the schematic representation (figure 4(c)). The interplanar distances of the outer part of the particle measured in figure 4(b) are consistent with the (400) $CoFe_2O_4$ planes. It is noteworthy that while the residual organic compound used in the synthesis isolates from each other the particles of the S1 and S2 systems, the S3 presents aggregates formed by a small number of nanoparticles, leading to a 'flower-like' morphology of 22 nm mean size. This feature was observed previously [27–29] and could be attributed to the lower surfactant/precursor molar ratio employed, which could favor

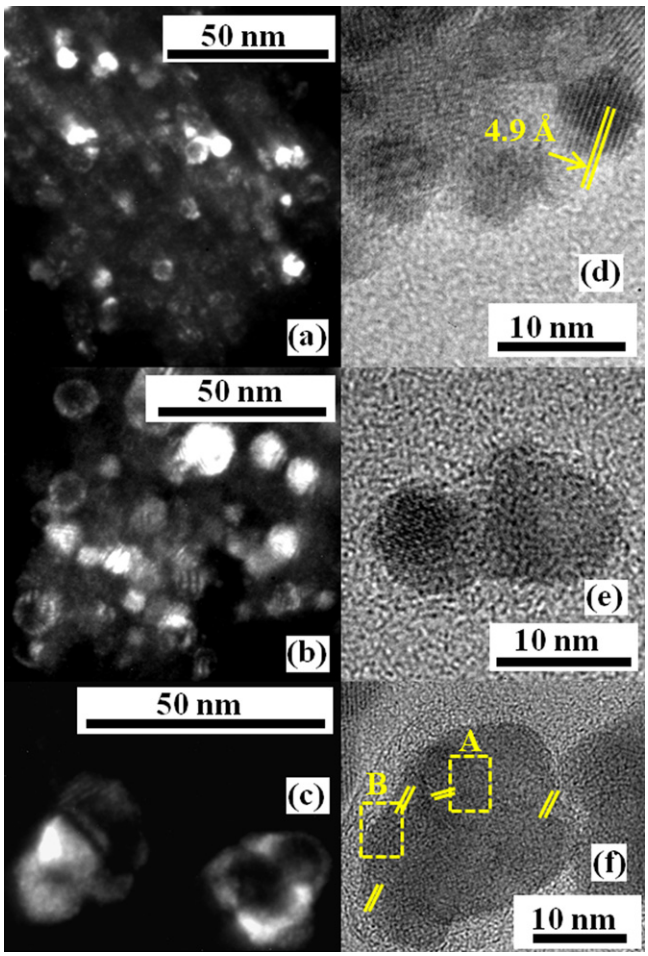

Figure 3. Dark-field TEM images of the S1, S2 and S3 CoO-core/$CoFe_2O_4$-shell samples ((a), (b) and (c), respectively), reconstructed with a fraction of the (111) $CoFe_2O_4$ electron diffraction ring. On the right, the HRTEM images of S1, S2 and S3 ((d), (e) and (f), respectively) are presented. The interplanar distances that correspond to the (111) $CoFe_2O_4$ plane are signaled (d), and different planes' orientations are pointed out for the inner -A- and outer part -B- of the particle (f); see figure 4 for further details.

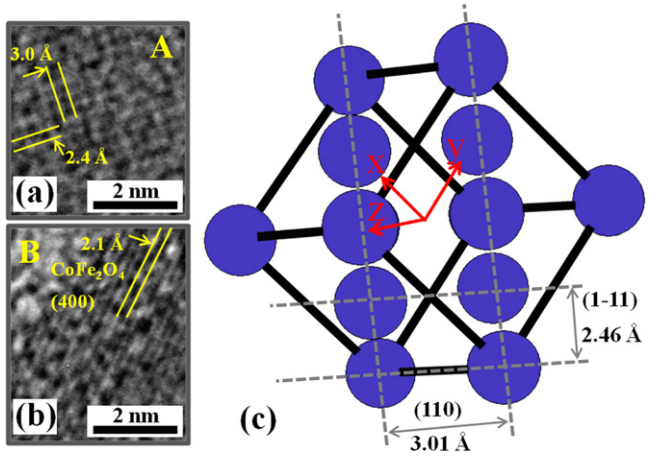

Figure 4. Details A (a) and B (b) of the S3 HRTEM image; the measured interplanar distances are indicated in each case. A schematic representation of the projection of the Co atoms in the CoO with the Fm3m structure along the [−112] direction (c), where planes (1–11) and (110) are indicated with its associated interplanar distances.

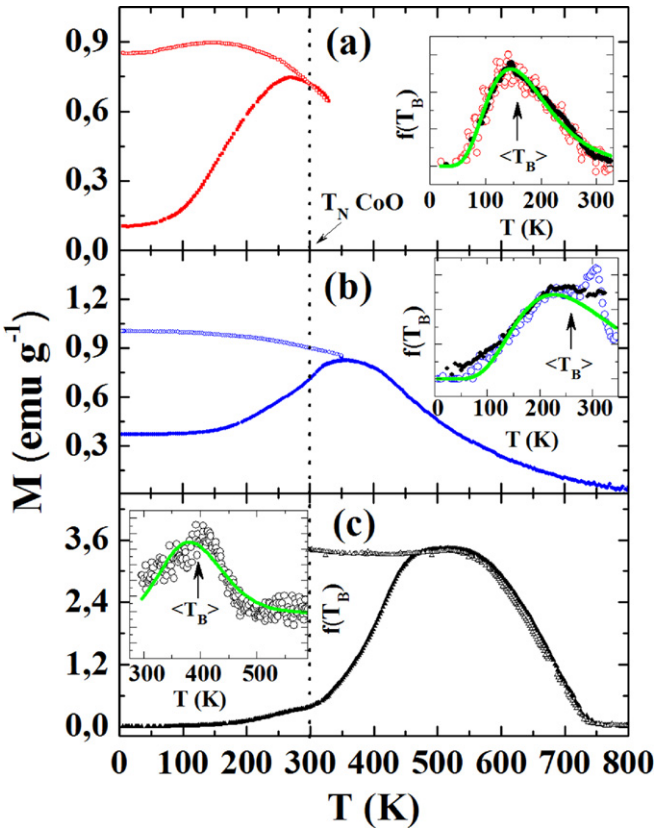

Figure 5. Temperature dependence of the ZFC and FC magnetization of the CoO-core/$CoFe_2O_4$-shell nanoparticles of samples S1, S2 and S3 ((a), (b) and (c), respectively). The insets show the distribution of energy barriers $f(T_B)$, calculated from the ZFCFC (empty dots) and TRM (full dots) measurements.

the agglomeration during the synthesis. In order to confirm the nature of the shell phase, we obtained dark-field TEM images recorded with a small objective aperture positioned on the inner electron diffraction ring (111) of the $CoFe_2O_4$ phase (figures 3(a)–(c)). Therefore, the bright contrast in the reconstructed images corresponds to the $CoFe_2O_4$ spinel phase, and a shell thickness of 1.3 nm, 2.2 nm and 2.6 nm for S1, S2 and S3, respectively, could be estimated.

Notice that the $CoFe_2O_4$ size determined from the XRD is larger than the one obtained by TEM. To understand these results, it should be remarked that from the XRD curves, the crystallite volume is estimated, while the TEM images give information about the shell thickness of the core/shell structure. In addition, figure 3 reveals that the $CoFe_2O_4$ crystallites grow up in the shell with a preferential orientation over the CoO seed, which could also result in a bigger XRD crystallite size. This feature was also observed in other core/shell systems and in hollow nanoparticles [23, 30].

3.2. Magnetic properties

The temperature dependences of the zero field cooling (ZFC) and field cooling (FC) magnetization are presented in figure 5. Measurements up to 330 K and above 300 K were carried out

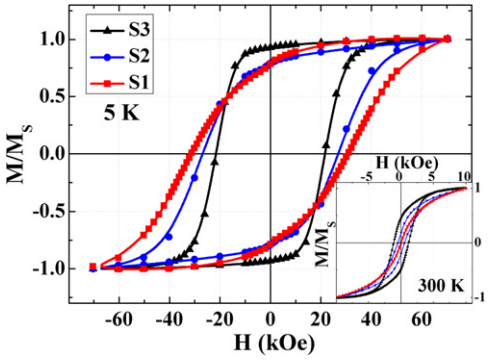

Figure 6. Hysteresis cycles measured at 5 K and 300 K (inset) for $CoO/CoFe_2O_4$ nanoparticles of different sizes.

in a SQUID magnetometer and a Faraday balance, respectively, and the results were normalized according to the mass employed in each experiment. The general feature of the M vs T curves is similar for the three samples. The magnetization is reversible at high temperatures, which is consistent with superparamagnetic behaviour; when the temperature diminishes, the ZFC and FC curves split, indicating that the nanoparticles' system is partially blocked, according to their effective magnetic anisotropy distribution. Another feature to remark on from figure 5 is the weak anomaly observed in the ZFC curve at around 300 K for the S2 and S3 samples. This anomaly could be related to the Néel temperature of the bulk CoO ($T_N \sim$ 293 K) [31, 32]. The ZFC curves show a maximum that shifts to higher temperatures when the size increases, i.e., $T_{MAX} \sim 270$ K (S1), 358 K (S2) and 508 K (S3). The energy barrier distribution from the ZFC and FC magnetization curves was calculated according to:

$$f\left(T_B\right) \propto (1/T)\left[\mathrm{d}\left(M_{ZFC} - M_{FC}\right)/\mathrm{d}T\right]. \quad (1)$$

It is known that the energy barrier distribution can also be obtained from the temperature decay of the remanence curve (TRM), according to $f\left(T_B\right) \propto (1/T)\left[\mathrm{d}M_{TRM}/\mathrm{d}T\right]$. The insets of figure 5 show $f(T_B)$, where an excellent agreement between both estimations can be observed. From the lognormal fits of $f(T_B)$, in the insets of figure 5, the $<T_B>$ was determined as the median value of the distribution. We found that when the nanoparticles' size grows, $<T_B>$ increases from 167 K to 271 K to 388 K for S1, S2 and S3, respectively. It is noteworthy that the blocking temperatures of the present core/shell nanoparticles are larger than those reported for $CoFe_2O_4$ single-phase nanoparticles of comparable size: $<T_B> \sim 23$ K, 48 K and 180 K for 2 nm, 3 nm and 5 nm $CoFe_2O_4$ nanoparticles [33], $<T_B> \sim 120$ K for 5 nm $CoFe_2O_4$ nanoparticles [34] and $<T_B> \sim 120$ K for $CoFe_2O_4$ with a similar shell morphology [24]. The comparison suggests that the larger $<T_B>$ values are due to the core/shell interface coupling, but the important role of the interparticle interactions on the enhancement of the thermal stability also has to be taken into account. Indeed, such interactions are clearly evidenced by the flattening of the FC magnetization curve below T_{MAX} [6].

In order to evaluate the magnetic hardening of the bimagnetic system, we have measured hysteresis cycles as a function of temperature. Figure 6 shows M vs H curves at 5 K for the three nanoparticle sizes. From this figure, a systematic increase of the coercive field H_C is observed when the size of the particles decreases; in fact, H_C changes from 21.5 kOe to 30.8 kOe when the size is reduced (see table 2). It is noteworthy that the coercive fields measured at a low temperature are higher than the one reported for single-phase $CoFe_2O_4$. The highest coercive field observed for $CoFe_2O_4$ at 10 K is around 20 kOe, as reported for 16 nm particles fabricated by the high-temperature organometallic decomposition method [35] and for 40 nm particles fabricated by seed-mediated growth-dominant coprecipitation [36]. In addition, the coercivity observed at 5 K for 7.5 nm $ZnO/CoFe_2O_4$ core/shell nanoparticles with a shell thickness of ~2 nm is $H_C \sim$ 7.8 kOe [24]. From these observations, we can conclude that the interface exchange interaction between the antiferromagnetic core and the ferrimagnetic shell plays a relevant role in the magnetic hardening of the system. When the temperature is raised, a fraction of the particles enters the superparamagnetic regime, according to their energy barrier distribution (insets of figure 5); as a consequence, the coercive field decreases. Notice that the smallest particles (S1) present a strong

Table 2. Magnetic properties: coercive fields (H_C) at 5 and 300 K, squareness ratio (M_R/M_S) and mean blocking temperature, calculated from ZFC-FC magnetization curves ($<T_B>$).

Sample	H_C 5 K (kOe)	H_C 300 K (kOe)	M_R/M_S 5 K	$<T_B>$ (K)
S1	30.8	0	0.77	167
S2	27.8	0.5	0.78	271
S3	21.5	1.1	0.93	388

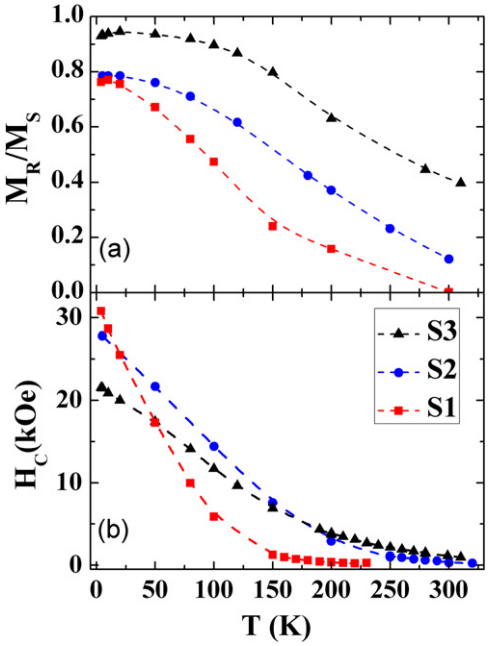

Figure 7. Temperature dependence of the squareness ratio (a) and temperature dependence of the coercive field (b) for $CoO/CoFe_2O_4$ nanoparticles of different sizes.

reduction of H_C up to 150 K (figure 7(b)), while the largest particles (S3) present a smoother temperature dependence. The size dependence of H_C shows an opposite behaviour at room temperature compared to the 5 K measurements, and the coercivity increases with size due to the largest fraction of still-blocked particle moments.

The temperature dependence of the remanence to the saturation magnetization ratio (M_R/M_S) is reported in figure 7(a). At a low temperature, the M_R/M_S ratio changes from 0.93 to 0.77 when the size is reduced. For the smallest particles (S1), M_R/M_S shows an important and more rapid reduction with the temperature, while larger particles (S2, S3) present a smoother dependence. Therefore, the ratios are 0, 0.1 and 0.4 for S1, S2 and S3 at room temperature, respectively.

It is noteworthy that no significant shift of the hysteresis loops is observed at 5 K after cooling from 320 K under different applied fields: between 20 and 40 kOe. The lack of an exchange bias can be ascribed to the comparable magnetic anisotropy of the two materials, as we will discuss later. Indeed, to observe the exchange bias, the anisotropy of the antiferromagnetic phase is requested to be larger than that of the ferro(ferri)magnetic phase. Moreover, the anisotropy energy of the antiferromagnet has to be larger than the interface exchange energy. The antiferromagnetic phase is only able to exert a pinning action on the magnetization of the ferro(ferri)magnet in the presence of both conditions.

3.3. Discussion and conclusions

The high-temperature decomposition of the organometallic compounds involves several parameters to be controlled, such as the heating rate, reflux temperature, reflux time and the molar ratio between the surfactants and precursors. After adjusting some of them, it is possible to obtain particles with different sizes and morphologies [37–39], which allow the fabrication of artificial nanostructures with controlled properties. In particular, we have designed and fabricated antiferromagnetic/ferrimagnetic core/shell nanoparticles, which show thermal stability improvement and hardening of the magnetic properties.

During the synthesis, the nucleation process takes place after the decomposition of the organometallic compounds, which increases the concentration of ions above the nucleation limit. A low heating rate leads to a more homogeneous decomposition process; consequently, a large amount of ions are used in the formation of a large number of nuclei. On the other hand, a high heating rate produces a less homogeneous decomposition, forming a smaller amount of nuclei and larger particles at the end of the synthesis. Our results are as follows: a lower heating rate produces smaller cores ($<D_{CORE}> \sim 3$ nm), while a higher one produces larger cores ($<D_{CORE}> \sim 6$ nm). Another advantage of the method is the as-formed organic coating of the nanoparticles that prevents their coalescence, allowing a subsequent thermal treatment that improves the crystallinity without a noticeable size growth. However, in the case of larger nanoparticles fabricated with a lower surfactant/precursor ratio, aggregates formed by a few nanoparticles were observed. Although the synthesis method employed in this work allows good control of the size, crystallinity and composition of the nanoparticles, it is limited by the total volume of the material that can be obtained. While many methods for the fabrication of monodisperse and shape-controlled nanocrystals have been studied [40], e.g., thermal decomposition of metal-surfactant complexes, nonhydrolytic sol–gel or polyol processes, the production of core/shell nanoparticles, particularly when a multistep method is required, increases the complexity [41], and full parameterization of the synthesis processes is needed. Although some advances in the development of large-scale single-reaction methods involving nontoxic and inexpensive reagents have been done [42], achieving scalability to a desired commercial scale is still a challenge.

The overall magnetic measurements show that CoO/$CoFe_2O_4$ bimagnetic nanoparticles present an enhancement of the thermal stability and magnetic hardening, as compared to their single-phase $CoFe_2O_4$ counterparts. $CoFe_2O_4$ nanoparticles with different morphologies and concentrations were extensively studied [34–36, 43], and none of these systems surpass a coercive field of 20 kOe at low temperature. In our case, the H_C increases up to 30 kOe in the smallest core/shell system (S1), and the origin of such magnetic hardening is associated to the strong FiM/AFM interface exchange interaction [24].

Thermal stability of exchange biased systems is associated with magnetic anisotropy of the AFM grains. Conventionally, the blocking temperature in exchange-coupled bimagnetic systems is defined as the temperature at which the exchange bias field, H_{EB}, goes to zero [44, 45]. In this situation, following the analysis of Fulcomer and Charap [46], the AFM core has to overcome the energy barrier given by $E_{AFM} = K_{AFM}V_{AFM}\sin^2\alpha - J_{INT}\cos\alpha$, where K_{AFM} and V_{AFM} are the magnetic anisotropy constant and the magnetic volume of the AFM phase, J_{INT} is the exchange coupling constant at the interface, and α is the angle between the easy axis of the AFM and its magnetization. In this model, $K_{AFM}V_{AFM} \geqslant J_{INT}$ and the energy barrier vanishes when $K_{AFM}V_{AFM} = J_{INT}$; as a consequence, the shift of the magnetization loop is no longer observed. The situation regarding the CoO/$CoFe_2O_4$ bimagnetic system is different because it does not present a shift of the hysteresis cycle but an enhancement of the coercive field, indicating that the FiM and AFM spins are strongly coupled at the interface ($K_{AFM}V_{AFM} \ll J_{INT}$). In this limit, the energy barrier for a strongly coupled system could be expressed as [24]:

$$E = -\left(Hm_{FiM}V_{FiM} + Hm_{AFM}V_{AFM}\right)\cos(\theta - \alpha) + \left(K_{FiM}V_{FiM} + K_{AFM}V_{AFM}\right)\sin^2(\alpha) \quad (2)$$

where H is the applied magnetic field; m_{FiM} is the FiM magnetization, normalized by the total FiM volume (V_{FiM}); m_{AFM} is the uncompensated AFM magnetization, normalized by the total AFM volume (V_{AFM}); K_{FiM} is the magnetic anisotropy of the FiM; α is the angle between m_{AFM}, m_{FiM} and the easy axis direction; θ is the angle between H and the easy axis direction. According to the theory of

superparamagnetism, the relaxation time τ varies exponentially with the energy barrier, so by taking equation (2) into account, we can define the blocking temperature of the exchange-coupled core/shell nanoparticles at zero field from:

$$\Delta E = K_{\mathrm{FiM}} V_{\mathrm{FiM}} + K_{\mathrm{AFM}} V_{\mathrm{AFM}} = \ln\left(\tau_{\mathrm{M}}/\tau_0\right) k_{\mathrm{B}} \left\langle T_{\mathrm{B}} \right\rangle, \quad (3)$$

where $\tau_{\mathrm{M}} \sim 100$ s and $\tau_0 \sim 10^{-9}$ s are the measurement time and the characteristic relaxation time of the material, respectively, and k_{B} is the Boltzmann constant. From the free energy expressed in equation (2), the coercive field at $T = 0$ K of an AFM/FiM coupled system of randomly oriented particles can be obtained:

$$\begin{aligned} H_{\mathrm{C}} &= 0.96\left(K_{\mathrm{FiM}} V_{\mathrm{FiM}} + K_{\mathrm{AFM}} V_{\mathrm{AFM}}\right)/\left(m_{\mathrm{FiM}} V_{\mathrm{FiM}} \right. \\ &\quad \left. + m_{\mathrm{AFM}} V_{\mathrm{AFM}}\right) \\ &\cong 0.96\left(K_{\mathrm{FiM}}/m_{\mathrm{FiM}} + K_{\mathrm{AFM}} V_{\mathrm{AFM}}/m_{\mathrm{FiM}} V_{\mathrm{FiM}}\right). \end{aligned} \quad (4)$$

Notice that the above oversimplified model of the core/shell nanoparticle system describes the observed size dependence of $<T_{\mathrm{B}}>$ and H_{C} well. While the blocking temperature increases with the volume of the magnetic phases (weighted by their anisotropy constant), the magnetization reversal is governed by the AFM/FiM volume proportion. These equations are consistent with the results reported for the exchange coupled AFM/FiM films, where the coupling is more effective when the film thickness diminishes [31, 47, 48]. In order to evaluate the predicted $<T_{\mathrm{B}}>$ and H_{C} from equations (3) and (4) for the CoO/$CoFe_2O_4$ bimagnetic nanoparticles, an estimation of the magnetic volumes should be performed. In the previous section, we pointed out that the ferrite shell does not grow uniformly over the core but is formed by a number of partially aligned nanocrystals. According to the TEM measurements, it is possible to consider that each AFM core is coupled to ~4–5 grains that occupy the total volume of the shell. Within this approximation, $<T_{\mathrm{B}}>$ resulted in 121 K and 403 K for S1 and S2, respectively. On the other hand, $<T_{\mathrm{B}}>$ of S3 is clearly above the CoO Néel temperature, so only the magnetic anisotropy of the FiM phase should be considered. Furthermore, in this last case, the energy barrier is increased by the interparticle interactions promoted by the nanoparticle agglomeration. By employing equation (4), we can estimate the coercivity as a function of the size for a random spatial distribution of anisotropy easy axes. These values were calculated using the magnetic anisotropy constants $K_{\mathrm{AFM}} \sim 4 \cdot 10^7$ erg cm^{-3} [24] and $K_{\mathrm{FiM}} \sim 4 \cdot 10^6$ erg cm^{-3} [24, 49], along with the bulk ferrimagnetic magnetization of $CoFe_2O_4$ $m_{\mathrm{FiM}} \sim$ 424 emu cm^{-3} and the volumes estimated by TEM. The coercive fields resulted in ~68 kOe, ~49 kOe and ~31 kOe for S1, S2 and S3, respectively. As we mentioned above, this simple approach describes the tendency observed in the studied systems well, although the calculated H_{C} values are overestimated. The discrepancy could be due mainly to oversimplification of the model, as, for example, it does not take into account interface imperfections and misalignment between the AFM/FiM anisotropy easy axes caused by the complex shell structure. In addition, it is worth noting that these models are based on the hypothesis of coherent rotation of the magnetization, which is only valid for systems with characteristic sizes smaller than the coherence radius $R_{\mathrm{COH}} \sim 5$–10 nm [50, 51]. Therefore, it is reasonable to apply the above phenomenological picture to the S1 and S2 samples because their characteristic sizes (cores sizes $\leqslant 3.8$ nm and shell $\leqslant 2.2$ nm) are smaller than R_{COH}. However, the more complex morphology of the larger S3 system implies that other factors, such as structural imperfections and bigger $CoFe_2O_4$ crystallite grains, could play a fundamental role in the reversal process.

Regarding the normalized remanent magnetization of the S1 and S2 systems, the low temperature $M_{\mathrm{R}}/M_{\mathrm{S}}$ values are closer to the theoretical value predicted for non-interacting spatially randomly oriented nanoparticles with cubic magnetic anisotropy ($M_{\mathrm{R}}/M_{\mathrm{S}} = 0.83$) than to the value reported for uniaxial anisotropy ($M_{\mathrm{R}}/M_{\mathrm{S}} = 0.5$) [52]. This result suggests that the $CoFe_2O_4$ shell presents cubic anisotropy, even with a thickness as thin as ~1.3 nm, in contrast to what was reported for the $CoFe_2O_4$ single-phase nanoparticles [20, 33, 43]. It could be assumed that the overgrowth of the $CoFe_2O_4$ shell over the CoO core diminishes the crystalline and magnetic surface disorder of the $CoFe_2O_4$ phase, leading to a highly crystalline FiM phase with cubic anisotropy, even when the shell thickness is about 1–2 nm. It can also be remarked that S3 shows a high $M_{\mathrm{R}}/M_{\mathrm{S}}$ ratio of >0.8 up to 150 K, even though the coercivity at that temperature is reduced to a third of the low temperature value. Such high $M_{\mathrm{R}}/M_{\mathrm{S}}$ values cannot be explained just by considering cubic magnetocrystalline anisotropy for $CoFe_2O_4$. In our case, the sample S3 was formed by core/shell particles in close contact, supporting the possibility of an exchange coupling between the particles that form the nano-aggregates. In the remanent state, and after saturation by a large magnetic field, a significant number of nanoparticle surface magnetic moments could deviate from their easy axis toward the applied magnetic field direction due to the competition between the magnetocrystalline anisotropy and the interparticle exchange interaction. As a consequence, the resultant spontaneous polarization in the field direction would be higher compared with the remanent magnetization of the non-interacting particles. This behaviour is supported by theoretical and experimental studies in nanoparticles and nanocomposites [10, 53, 54]. On the other hand, despite the fact that magnetic stability can be increased by magnetic coupling up to the ordering temperature of the antiferromagnetic phase, the magnetic properties of all of the samples are strongly diminished when the temperature is increased due to their reduced sizes. Therefore, further strategies, e.g, employing an antiferromagnetic material with a T_{N} that is much higher than room temperature, should be investigated in order to design new materials suitable for commercial uses.

In summary, we have shown that the control of the dimensions and morphology of bimagnetic core/shell nanoparticles in the nanoscale is a very powerful way to design new materials with optimized properties. When the nanoparticle size is reduced, the system presents a remarkable increase of the magnetic hardening due to the enhancement of the magnetic anisotropy by the interface exchange interaction. We have demonstrated that the core/shell morphology favours

the formation of a highly crystalline magnetic phase, which improves the coupling at the interface. However, the energy barrier associated to the magnetocrystalline anisotropy decreases when the nanoparticle size is reduced, and the system loses its thermal stability more rapidly with an increasing temperature. In conformity, the coercivity and the M_R/M_S ratio fall rapidly when the temperature is increased. By applying a simple phenomenological model to the bimagnetic nanoparticles' system, it is possible to explain the main size effects reflected by the magnetic measurements. Finally, we conclude that the effective magnetic anisotropy can be raised by reducing the characteristic size of the FiM and AFM phases and by improving the quality of the interface of the bimagnetic nanoparticles.

Acknowledgments

The authors thank ANPCyT Argentina through Grant PICT 2007-0832, CONICET Argentina through Grant PIP 2008-1333 and UNCuyo Argentina through Grants 06-C404 and 06-C011.

References

[1] Aktas B, Tagirov L and Mikhailov F 2007 *Magnetic Nanostructures* (Berlin: Springer-Verlag)
[2] Sellmyer D and Skomski R 2006 *Advanced Magnetic Nanostructures* (New York: Springer)
[3] Schmid G 2004 *Nanoparticles: From Theory to Application* (Weinheim: Wiley-VHC)
[4] Balamurugan B, Sellmyer D J, Hadjipanayis G C and Skomski R 2012 Prospects for nanoparticle-based permanent magnets *Scr. Mater.* **67** 542–7
[5] Skumryev V, Stoyanov S and Zhang Y 2003 Beating the superparamagnetic limit with exchange bias *Nature* **423** 19–22
[6] Dormann J L, Fiorani D and Tronc E 1997 Magnetic relaxation in fine-particle systems *Advanced in Chemical Physics Vol XCVIII* (New York: Wiley)
[7] Kodama R 1999 Magnetic nanoparticles *J. Magn. Magn. Mater.* **200** 359–72
[8] Nandwana V, Chaubey G S, Yano K, Rong C and Liu J P 2009 Bimagnetic nanoparticles with enhanced exchange coupling and energy products *J. Appl. Phys.* **105** 014303
[9] Jones N 2011 Materials science: the pull of stronger magnets *Nature* **472** 22–3
[10] Sort J, Nogués J, Suriñach S, Muñoz J S, Baró M D, Chappel E, Dupont F and Chouteau G 2001 Coercivity and squareness enhancement in ball-milled hard magnetic–antiferromagnetic composites *Appl. Phys. Lett.* **79** 1142
[11] Liu F, Zhu J, Yang W, Dong Y, Hou Y, Zhang C, Yin H and Sun S 2014 Building nanocomposite magnets by coating a hard magnetic core with a soft magnetic shell *Angew. Chem. Int. Ed. Engl.* **53** 2176–80
[12] Sun S, Murray C, Weller D, Folks L and Moser A 2000 Monodisperse FePt nanoparticles and ferromagnetic FePt nanocrystal superlattices *Science* **287** 1989–92
[13] Hyeon T, Lee S S, Park J, Chung Y and Na H B 2001 Synthesis of highly crystalline and monodisperse maghemite nanocrystallites without a size-selection process *J. Am. Chem. Soc.* **123** 12798–801
[14] Bodnarchuk M I, Kovalenko M V, Groiss H, Resel R, Reissner M, Hesser G, Lechner R T, Steiner W, Schäffler F and Heiss W 2009 Exchange-coupled bimagnetic wüstite/metal ferrite core/shell nanocrystals: size, shape, and compositional control *Small* **5** 2247–52
[15] Peng S, Xie J and Sun S 2008 Synthesis of Co/MFe_2O_4 (M = Fe, Mn) core/shell nanocomposite particles *J. Solid State Chem.* **181** 1560–4
[16] Zeng H, Sun S, Li J, Wang Z L and Liu J P 2004 Tailoring magnetic properties of core/shell nanoparticles *Appl. Phys. Lett.* **85** 792
[17] Salazar-Alvarez G, Lidbaum H, López-Ortega A, Estrader M, Leifer K, Sort J, Suriñach S, Baró M D and Nogués J 2011 Two-, three-, and four-component magnetic multilayer onion nanoparticles based on iron oxides and manganese oxides *J. Am. Chem. Soc.* **133** 16738–41
[18] López-Ortega A *et al* 2010 Size-dependent passivation shell and magnetic properties in antiferromagnetic/ferrimagnetic core/shell MnO nanoparticles *J. Am. Chem. Soc.* **132** 9398–407
[19] Masala O and Seshadri R 2005 Spinel ferrite/MnO core/shell nanoparticles: chemical synthesis of all-oxide exchange biased architectures *J. Am. Chem. Soc.* **127** 9354–5
[20] Leite G C P, Chagas E F, Pereira R, Prado R J, Terezo A J, Alzamora M and Baggio-Saitovitch E 2012 Exchange coupling behavior in bimagnetic $CoFe_2O_4$/$CoFe_2$ nanocomposite *J. Magn. Magn. Mater.* **324** 2711–6
[21] Soares J M, Cabral F A O, de Araújo J H and Machado F L A 2011 Exchange-spring behavior in nanopowders of $CoFe_2O_4$–$CoFe_2$ *Appl. Phys. Lett.* **98** 072502
[22] Estrader M *et al* 2013 Robust antiferromagnetic coupling in hard-soft bi-magnetic core/shell nanoparticles *Nat. Commun.* **4** 2960
[23] Lima E, Winkler E L, Tobia D, Troiani H E, Zysler R D, Agostinelli E and Fiorani D 2012 Bimagnetic CoO Core/$CoFe_2O_4$ shell nanoparticles: synthesis and magnetic properties *Chem. Mater.* **24** 512–6
[24] Winkler E L, Lima E, Tobia D, Saleta M E, Troiani H E, Agostinelli E, Fiorani D and Zysler R D 2012 Origin of magnetic anisotropy in ZnO/$CoFe_2O_4$ and CoO/$CoFe_2O_4$ core/shell nanoparticle systems *Appl. Phys. Lett.* **101** 252405
[25] Rodríguez-Carvajal J 1993 Recent advances in magnetic structure determination by neutron powder diffraction *Phys. B Condens. Matter* **192** 55
[26] León-Félix L, Chaker J, Parise M, Coaquira J A H, Santos Valladares L, Bustamante A, Garg V K, Oliveira A C and Morais P C 2013 Synthesis and characterization of uncoated and gold-coated magnetite nanoparticles *Hyperfine Interact.* **224** 179–88
[27] Chen Z, Xu A, Zhang Y and Gu N 2010 Preparation of NiO and CoO nanoparticles using M^{2+}-oleate (M = Ni, Co) as precursor *Curr. Appl. Phys.* **10** 967–70
[28] Niederberger M and Pinna N 2009 *Metal Oxide Nanoparticles in Organic Solvents* (London: Springer)
[29] Wang H, Si H, Zhao H, Du Z and Li L S 2010 Shape-controlled synthesis of cobalt oxide nanocrystals using cobalt acetylacetonate *Mater. Lett.* **64** 408–10
[30] Lima E, Vargas J M, Zysler R D, Rechenberg H R, Cohen R, Arbiol J, Goya G F, Ibarra A and Ibarra M R 2009 Single-step chemical synthesis of ferrite hollow nanospheres *Nanotechnology* **20** 045606
[31] Nogués J and Schuller I K 1999 Exchange bias *J. Magn. Magn. Mater.* **192** 203–32
[32] Goodenough J 1971 Metallic oxides *Prog. Solid State Chem.* **5** 145–399
[33] Moumen N and Pileni M P 1996 Control of the size of cobalt ferrite magnetic fluid *J. Phys. Chem.* **100** 1867–73
[34] Peddis D, Orrù F, Ardu A, Cannas C, Musinu A and Piccaluga G 2012 Interparticle interactions and magnetic

anisotropy in cobalt ferrite nanoparticles: influence of molecular coating *Chem. Mater.* **24** 1062–71
[35] Sun S, Zeng H, Robinson D B, Raoux S, Rice P M, Wang S X and Li G 2004 Monodisperse MFe_2O_4 (M = Fe, Co, Mn) nanoparticles *J. Am. Chem. Soc.* **126** 273–9
[36] Chinnasamy C N, Jeyadevan B, Shinoda K, Tohji K, Djayaprawira D J, Takahashi M, Joseyphus R J and Narayanasamy A 2003 Unusually high coercivity and critical single-domain size of nearly monodispersed $CoFe_2O_4$ nanoparticles *Appl. Phys. Lett.* **83** 2862
[37] Hyeon T 2003 Chemical synthesis of magnetic nanoparticles *Chem. Commun.* **2003** 927–34
[38] Guardia P, Pérez-Juste J, Labarta A, Batlle X and Liz-Marzán L M 2010 Heating rate influence on the synthesis of iron oxide nanoparticles: the case of decanoic acid *Chem. Commun.* **46** 6108–10
[39] Vargas J M and Zysler R D 2005 Tailoring the size in colloidal iron oxide magnetic nanoparticles *Nanotechnology* **16** 1474–6
[40] Park J, Joo J, Kwon S G, Jang Y and Hyeon T 2007 Synthesis of monodisperse spherical nanocrystals *Angew. Chem. Int. Ed. Engl.* **46** 4630–60
[41] Ghosh Chaudhuri R and Paria S 2012 Core/shell nanoparticles: classes, properties, synthesis mechanisms, characterization, and applications *Chem. Rev.* **112** 2373–433
[42] Park J, An K, Hwang Y, Park J-G, Noh H-J, Kim J-Y, Park J-H, Hwang N-M and Hyeon T 2004 Ultra-large-scale syntheses of monodisperse nanocrystals *Nat. Mater.* **3** 891–5
[43] Peddis D *et al* 2013 Beyond the effect of particle size: influence of $CoFe_2O_4$ nanoparticle arrangements on magnetic properties *Chem. Mater.* **25** 2005–13
[44] Xi H, White R M, Gao Z and Mao S 2002 Antiferromagnetic thickness dependence of blocking temperature in exchange coupled polycrystalline ferromagnet/antiferromagnet bilayers *J. Appl. Phys.* **92** 4828
[45] O'Grady K, Fernandez-Outon L E and Vallejo-Fernandez G 2010 A new paradigm for exchange bias in polycrystalline thin films *J. Magn. Magn. Mater.* **322** 883–99
[46] Fulcomer E and Charap S H 1972 Thermal fluctuation aftereffect model for some systems with ferromagnetic-antiferromagnetic coupling *J. Appl. Phys.* **43** 4190
[47] Radu F and Zabel H 2008 *Magnetic Heterostructures* (*Springer Tracts in Modern Physics* vol 227) (Berlin: Springer) doi:10.1007/978-3-540-73462-8
[48] Seu K, Huang H, Lesoine J F, Showman H D, Egelhoff W F, Gan L and Reilly C 2003 Co layer thickness dependence of exchange biasing for IrMn/Co and FeMn/Co *J. Appl. Phys.* **93** 6611
[49] O'Handley R 1999 *Modern Magnetic Materials: Principles and Applications* (New Jersey: Wiley)
[50] Skomski R 2003 Nanomagnetics *J. Phys. Condens. Matter* **15** R841–96
[51] Cullity B D and Graham C D 2009 *Introducion to Magnetic Materials* (New Jersey: Wiley)
[52] Chikazumi S 1999 *Physics of Ferromagnetism* (New York: Oxford University Press)
[53] Du H F and Du A 2007 Effect of exchange and dipolar interactions on the hysteresis of magnetic nanoparticle systems *Phys. Status Solidi* **244** 1401–8
[54] Schrefl T, Fidler J and Kronmüller H 1994 Remanence and coercivity in isotropic nanocrystalline permanent magnets *Phys. Rev.* B **49** 6100–10